J. Fluid Mech. (1991), *vol.* 228, *pp.* 87–109
Printed in Great Britain

Resistance of a grooved surface to parallel flow and cross-flow

By PAOLO LUCHINI, FERNANDO MANZO AND AMILCARE POZZI

Istituto di Gasdinamica, Facoltà di Ingegneria, University of Naples, Italy

(Received 8 November 1990)

A study is undertaken of both parallel flow and cross-flow in the viscous sublayer generated by a fluid streaming along a grooved surface, with the aim of clarifying the phenomena that underlie the reduction of turbulent drag by such surfaces. A quantitative characterization of the effectiveness of different groove profiles in retarding secondary cross-flow is given in terms of the difference of two 'protrusion heights'. Analytical calculations of limit cases and a boundary-element computer code for the analysis of general profiles are illustrated, and several examples are presented and discussed.

1. Introduction

1.1. *Drag reduction by means of grooved surfaces*

In the quest for drag reduction in internal and external flows three methods seem to be the major contenders today (Bushnell 1983; Trigui & Guezennec 1990): delaying separation of the boundary layer by triggering an early transition to turbulent flow or otherwise affecting the boundary layer by injection or suction of fluid; modifying the viscosity of the fluid in the boundary layer by injection of a suitable different fluid or by changing its temperature; and shaping the wall with grooves (or riblets, depending on the way one wishes to see them) cut along the main flow direction.

Of these methods the first is technologically the most advanced, having been in use for a long time in airplane wings in at least some form; and the second has been proposed mainly for internal flows, such as the transportation of very viscous fluids in long pipelines (Preziosi, Chen & Joseph 1989, and references therein), its application to external flows being considered too costly. Both are quite clearly understood in their basic mechanism.

The third method, corrugating the surface, is very appealing because of its completely passive nature, but its mechanism of operation is much less well understood, and in fact one may even wonder, *a priori*, why it should reduce drag at all. Nevertheless, the observation that such corrugations occur naturally in shark scales (Burdak 1969; Chernyshov & Zayets 1970) triggered the interest of fluid-dynamicists in such structures, and in recent years it was experimentally shown (e.g. Bechert, Hoppe & Reif 1985; Sawyer & Winter 1987; Choi 1987; McLean, George-Falvy & Sullivan 1987) that a reduction of 4–7% compared to the drag of a smooth surface can indeed be achieved in turbulent flow. In addition, a qualitative explanation of the mechanism of drag reduction near grooved surfaces has gradually emerged (Bechert *et al.* 1985, 1986; Bechert & Bartenwerfer 1989; Baron, Quadrio & Vigevano 1989): the corrugations interfere with the secondary cross-flow associated with the longitudinal vortices which randomly appear in the turbulent flow, and

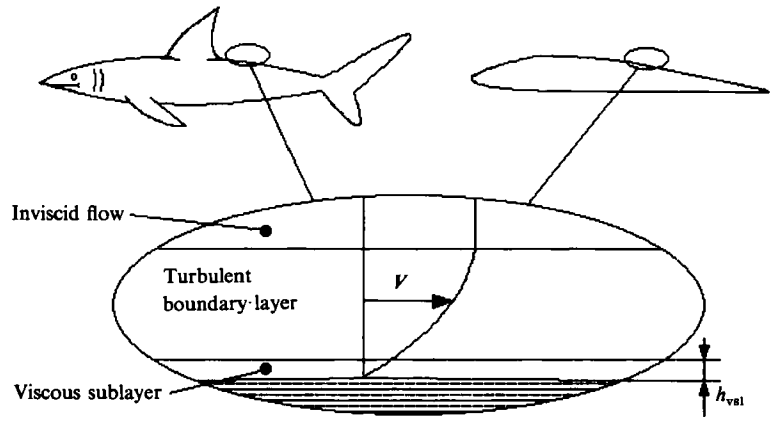

FIGURE 1. The phenomenon of drag reduction in a turbulent boundary layer, be it on shark skin or aeroplane wings, is produced by grooves (or riblets) interacting with the viscous sublayer.

somehow manage to dampen these vortices and therefore the level of turbulence itself; the consequent reduction in the rate of turbulent diffusion makes for a lower eddy viscosity and the reduction of drag.

Although the foregoing argument is intuitively convincing, it is only qualitative. However, the route to a deeper understanding of the effects of grooved surfaces is opened by Bechert's observation that the typical size of corrugations which appear to be experimentally effective is of the same order of magnitude as the height of the viscous sublayer of the turbulent stream (figure 1). Within the viscous sublayer, convective terms in the Navier–Stokes equations are negligible compared to the viscous terms, and therefore the flow can be studied in the much simpler framework of the Stokes equations. Bechert & Bartenwerfer (1989) studied in this way the alterations to the mean longitudinal flow produced by the corrugations. They argued that the velocity profile, which is asymptotically linear in the adjacent shear layer, appears as if it originated from an equivalent plane wall located at a distance below the riblet tips which they call the 'protrusion height', and were able to calculate the protrusion height of a number of riblet configurations for which the Laplace equation can be solved by conformal mapping.

Since, for all effects concerning the mean flow of the driving shear layer, the corrugated wall is equivalent to a suitably positioned plane wall, the resistance to the main flow is not automatically increased by the corrugations, as one might at first be led to believe; if the riblets do produce the effect of damping cross-flow and thus secondary streamwise vortices, the resistance may even be reduced, as it in practice is. Previous authors, however, have not quantitatively calculated the effect of the riblets on cross-flow.

1.2. *The unsteady viscous sublayer*

The mechanism of drag reduction by grooved surfaces outlined by Bechert and his collaborators relies on the influence that the corrugations have upon the unsteady fluctuations of the turbulent velocity field. It is therefore of the greatest importance to be able to describe and calculate this influence. This would be an almost hopeless task, at today's state of knowledge, without the previously mentioned observation that the most relevant phenomena take place inside the viscous sublayer of the turbulent stream. One can, therefore, expect to obtain useful information from a

study of the influence of the grooves on the unsteady viscous sublayer, which is governed by the linear Stokes equations.

In fact, an even greater simplification is possible. It occurred to one of us while listening to a review of the field by Baron *et al.* (1989) – which was a stimulus to start a research on this subject – that the Stokes equations for the unsteady flow in the viscous sublayer may be further simplified to the steady Stokes equations. The reason is simply that the inertia and convective terms of the Navier–Stokes equations are roughly of the same order of magnitude in a turbulent boundary layer, and therefore when the latter are negligible the former are too. We can thus delete time derivatives in the viscous-sublayer equations and study both mean flow and turbulent fluctuations by the steady (or quasi-steady, as they should more properly be called in such an application) Stokes equations. Of course, the fluctuating component *will* depend on time, but just because the boundary conditions for it do.

In further support for the assumption that useful results may be obtained while neglecting the time-derivative term in the Stokes equations even for the unsteady component of viscous-sublayer flow, we learnt from a referee, to whom we are indebted for his kindness, that Bechert's group also arrived at the same conviction. Bechert, Bartenwerfer & Hoppe (1990), after discussing at length the wave-like solutions of the unsteady Stokes equations, conclude, also on the basis of experimental measurements by other authors, that the frequencies typically encountered in turbulent flow are low enough for the viscous sublayer to be treated as quasi-steady. They, too, proceed to study the effects of riblets on cross-flow on the basis of the steady Stokes equations, and describe an analog device to obtain solutions of the biharmonic equation based on the deformation of an elastic thin plate with suitably constrained boundaries.

Bechert *et al.* (1990) also describe experiments conducted with a very viscous fluid on enlarged riblets for the purpose of measuring the difference between the resistance to parallel flow and cross-flow directly. We shall discuss their results later. It is important to note now, however, that they do find a larger resistance to cross- than to parallel flow and ascribe this difference to a different protrusion height.

1.3. *Past and present results*

Summarizing the state of the art in the description of flow near grooved surface we can say that:

(*a*) the phenomenon of turbulent drag reduction by grooved surfaces, experimentally verified by several authors, has been qualitatively explained (Bechert *et al.* 1985; Bechert & Bartenwerfer 1989; Baron *et al.* 1989);

(*b*) mean longitudinal flow in the viscous sublayer has been studied quantitatively, and the relevant parameter, the protrusion height, has been calculated for a number of groove shapes (including the limit of infinitely deep grooves), analytically by conformal mapping and analogically by simulation in an electrolytic tank (Bechert *et al.* 1986; Bechert & Bartenwerfer 1989).

(*c*) the effect of the grooves on low-Reynolds-number steady cross-flow has been studied experimentally and, in the quasi-steady approximation, through an analog simulation realized by bending a suitably constrained elastic thin plate. The cross-flow protrusion height has been measured during the simulation (Bechert *et al.* 1990).

This paper contains:

(*a*) a discussion of the transverse-flow problem insofar as it is relevant to the phenomenon of drag reduction and the mathematical definition of the transverse protrusion height (§§2 and 3);

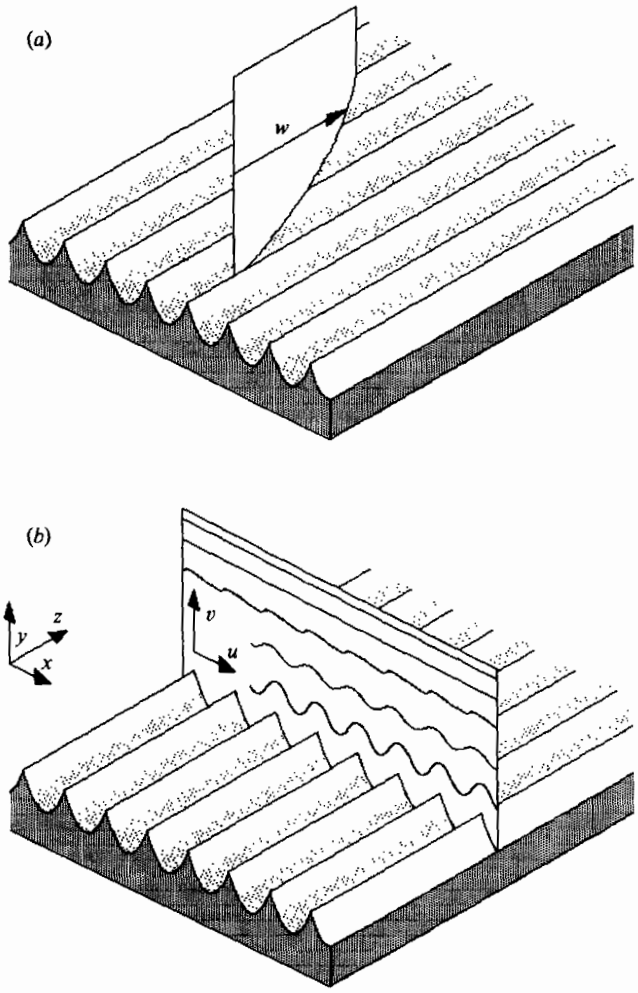

FIGURE 2. Schematic representation of (*a*) longitudinal, mean and turbulent, and (*b*) transverse, turbulent, flow over a grooved surface.

(*b*) the analytical solution of the transverse-flow problem in the limit of infinitely deep grooves and of the longitudinal- and transverse-flow problems in the limit of very shallow grooves (§4);

(*c*) the development of a boundary-element computer program that calculates the two protrusion heights of an arbitrary groove profile and the analysis by means of that program of the relative performance of various groove shapes (§§5 and 6).

2. Formulation of the problem

2.1. *Physical background*

The velocity profile in the boundary layer generated by flow of a fluid along a locally plane wall has at the wall end, where velocity is zero, a non-zero finite slope, related, as is well known, to the viscous shear stress in the fluid and to the friction drag acting on the wall itself. If one looks at the region near the wall on a scale small compared

to the boundary-layer thickness an approximately linear velocity profile with constant slope will be seen. This is the viscous sublayer (see figure 1), a region where the conversion of convected momentum into viscous stress is negligible with respect to the stress already present there, and the flow is governed mainly by the balance of viscous stresses. In other words, inertia and convective terms may be neglected in the Navier–Stokes equations and those equations may be reduced to the Stokes form.

Even in a turbulent stream we may expect the velocity profile to eventually become linear near the wall, with a slope approximately independent of the normal coordinate in a viscous sublayer of thickness

$$h_{\mathrm{vsl}} \approx (\nu/u_y)^{\frac{1}{2}} = (\nu^2\rho/\tau_{\mathrm{w}})^{\frac{1}{2}},$$

where ν is the kinematic viscosity of the fluid, ρ its density, u_y the slope of the velocity profile and τ_{w} the shear stress at the wall. (The latter quantity is more easily measurable in a turbulent flow because the velocity gradient will generally change in passing from the viscous sublayer to the truly turbulent boundary layer.) Notice, however, that in general u_y and τ_{w} will depend on time, keeping track of the unsteadiness of the turbulent eddies present in the boundary layer. Therefore the viscous sublayer, although governed by the linear and dissipative Stokes equations and therefore inherently stable, mirrors the time dependence of the shear layer that drives its motion.

Our aim in this paper is to study how flow in the viscous sublayer, in both the directions parallel and normal to the corrugations (see figure 2), is modified when the plane wall is replaced by a corrugated wall. Mathematically, the problem may be stated as follows.

2.2. *Mathematical formulation*

We wish to study the Stokes flow of a viscous fluid alongside an infinite corrugated wall in the presence of a given shear, or velocity gradient, in the region far from the wall. We shall assume the wall surface to be cylindrical, that is translation-invariant in one direction, which we shall take as z-axis, and periodic in a second direction normal to the first, which will be the x-axis. The direction normal to these two will be the y-axis. We shall also assume for the sake of simplicity, although this is not strictly necessary, that the surface does not bend over itself, so that it can be represented by an equation of the form $y = y_0(x)$ (where y_0 is independent of z and a periodic function of x). The equations we wish to solve are the Stokes equations:

$$\nabla \cdot \boldsymbol{V} = 0; \quad \nabla^2 \boldsymbol{V} = \mu^{-1} \nabla p, \tag{1}$$

with conditions specifying that the three components u, v, w (respectively along the x-, y- and z-axes) of velocity $\boldsymbol{V}$ be zero at the surface of equation $y = y_0(x)$, and that $\partial u/\partial y$ and $\partial w/\partial y$ should approach a given finite limit for y going to plus infinity.

It is easy to observe that, all quantities being independent of z, the equation for w decouples from the system and is just the Laplace equation

$$\nabla^2 w = 0 \tag{2a}$$

with boundary conditions

$$w[x, y_0(x)] = 0, \quad w_y(x, \infty) = \text{const.} \tag{2b}$$

(figure 3*a*). Equation (2*a*) with conditions (2*b*) is the problem that was studied by Bechert & Bartenwerfer (1989).

The transverse problem for the remaining unknowns u, v and p may be

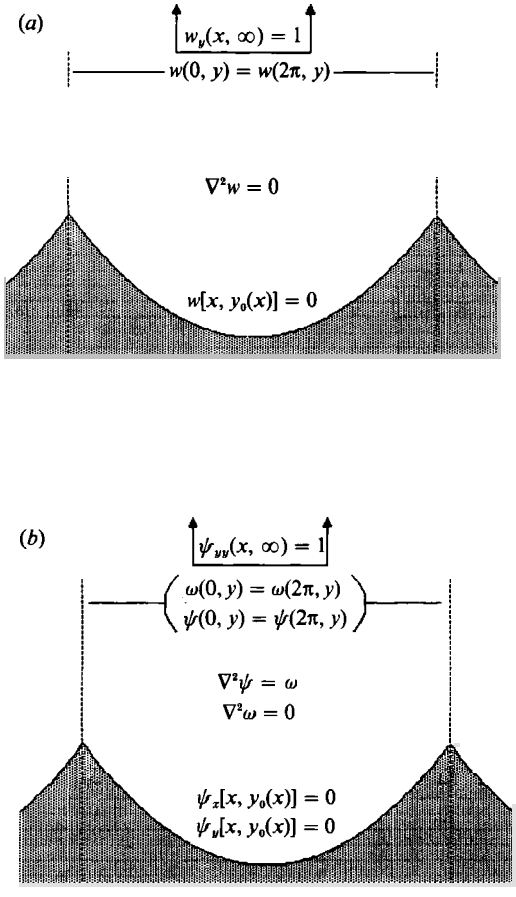

FIGURE 3. Geometry, equations and boundary conditions for (*a*) longitudinal and (*b*) transverse flow.

reformulated in terms of the stream function ψ, defined so that $\psi_y = u$ and $-\psi_x = v$, and of the vorticity $\omega = u_y - v_x$, by recasting (1) as

$$\nabla^2 \psi = \omega, \quad \nabla^2 \omega = 0, \tag{3a}$$

with boundary conditions

$$\psi_x[x, y_0(x)] = \psi_y[x, y_0(x)] = 0, \tag{3b}$$

$$\psi_{yy}(x, \infty) = \text{const.} \tag{3c}$$

(figure 3*b*). In the next section we shall see that these three conditions are indeed sufficient to identify a unique solution. In the meanwhile it is useful to remark that the two conditions stating that both ψ_x and ψ_y should vanish at the surface may be replaced by those that ψ itself be constant along the surface and that its directional derivative in any specified non-tangent direction should vanish there.

Finally, by suitably choosing a reference length and velocity (2) and (3) can always be non-dimensionalized in such a way that the period of the corrugations is 2π and the imposed velocity gradient at infinity is unity, and we shall assume so in most of the following.

3. The definition of protrusion height

The general solution of (2*a*) that is independent of z and periodic in x can be represented by a Fourier series of the form

$$w = \sum_{n=-\infty}^{\infty} W_n \mathrm{e}^{\mathrm{i}nx}, \tag{4a}$$

where

$$W_0 = a_0 + b_0 y \tag{4b}$$

and

$$W_n = a_n \mathrm{e}^{-|n|y} + b_n \mathrm{e}^{|n|y} \quad (n \neq 0). \tag{4c}$$

The condition that $w_y \to 1$ for $y \to +\infty$ fixes all the b-coefficients as $b_0 = 1$ and $b_n = 0$ for $n \neq 0$, and leaves the a-coefficients to be determined by the condition at the wall surface.

Since all the coefficients of the series (4*a*) but W_0 vanish exponentially at infinity, the solution obtained will approach the linear behaviour $w \sim a_0 + y$ with exponential accuracy, and thus imitate the velocity profile produced by a plane wall located at $y = -a_0$. Bechert's definition of the protrusion height $h_\parallel$ as the distance of the riblet tips, which he locates at $y = 0$, from this virtual origin of the velocity profile, may thus be rewritten as $h_\parallel = a_0$.

Notice that, from the standpoint of dimensional analysis, the protrusion height is a length, and therefore its dimensional value depends only on the chosen reference length and not on the reference velocity. The ratio of the protrusion height to the period of the corrugations, which we shall call normalized protrusion height $\bar{h}_\parallel$, is a purely geometrical parameter depending only on the shape of the wall corrugations and neither on their size nor on the actual speed of the driving fluid stream. As far as the main flow is concerned, the corrugated wall is equivalent to a plane wall located at a distance below the riblet tips which is given by the normalized protrusion height times the period.

We now want to show that a similar, but numerically different, protrusion height $h_\perp$ may be defined for the cross-flow as well. To this end we consider the Fourier series expansion of the general periodic solution of the biharmonic equation (3*a*), i.e.

$$\psi = \sum_{n=-\infty}^{\infty} \Psi_n \mathrm{e}^{\mathrm{i}nx}, \tag{5a}$$

where

$$\Psi_0 = A_0 + B_0 y + C_0 y^2 + D_0 y^3 \tag{5b}$$

and

$$\Psi_n = (A_n + B_n y)\mathrm{e}^{-|n|y} + (C_n + D_n y)\mathrm{e}^{|n|y} \quad (n \neq 0). \tag{5c}$$

The condition that $\psi_{yy} \to 1$ for $y \to \infty$ fixes all the C- and D-coefficients as $C_0 = \frac{1}{2}$, $D_0 = 0$ and $C_n = D_n = 0$ for $n \neq 0$, and leaves the A- and B-coefficients to be determined from the two conditions given at the wall surface. Just as in the previous case, the limiting behaviour $\psi \sim A_0 + B_0 y + \frac{1}{2}y^2$ is approached exponentially. The parallel velocity component $u = \psi_y \sim B_0 + y$ thus imitates the linear profile generated by a plane wall located at $y = -B_0$. The distance of the riblet tips from this virtual origin of the transverse velocity profile (which is different from the virtual origin of the longitudinal velocity profile) defines the transverse protrusion height $h_\perp = B_0$.

Just as in the previous case, for all effects concerning cross-flow in the driving turbulent shear layer, the corrugated wall is equivalent to a plane wall located at a distance below the riblet tips equal to the transverse protrusion height. If this virtual

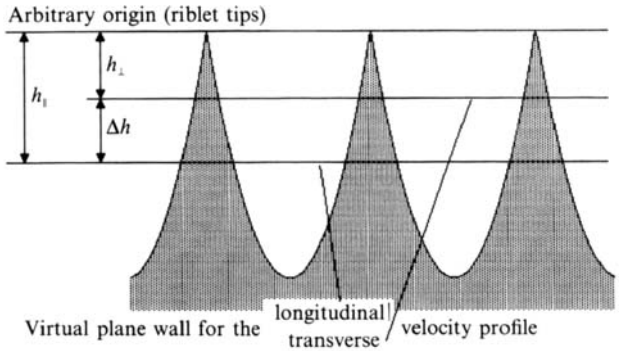

FIGURE 4. Interrelations between the protrusion heights and the positions of the virtual plane walls seen by longitudinal and transverse flow.

plane wall turns out to lie above the one seen by the longitudinal flow, that is if $h_\perp$ is smaller than $h_\parallel$, secondary cross-flow will experience a higher viscous dissipation, just as if it flowed in a narrower duct, than the main longitudinal flow, and the level of near-wall turbulence will presumably be reduced.

Once the two protrusion heights are defined, we arrive at the overall picture given in figure 4. The two protrusion heights represent the distances of the two virtual plane walls seen by the longitudinal and transverse flow respectively from the riblet tips. We may remark, however, that the riblet tips themselves do not hold any particular significance in relation to the flow, and must be considered for all purposes an arbitrary origin of the y-axis which has been set there just for geometrical convenience. It is evident that any physically significant parameter must be independent of the choice of the origin; the only combination of the two protrusion heights that has this property is their difference $\Delta h = h_\parallel - h_\perp$ (or functions thereof), i.e. the distance between the two virtual plane walls seen by longitudinal and transverse flow.

Δh gives a quantitative characterization of whether and how much the corrugated wall impedes the cross-flow more than it does the longitudinal flow, and is the only parameter on which the behaviour of the turbulent boundary layer may depend.

4. Analytical results

The problem of longitudinal flow over a wall with infinitely deep grooves (which reduces to an array of infinitely thin blades) was solved by Bechert & Bartenwerfer (1989) by conformal mapping. In this section we give the solution for both longitudinal and transverse flow over very shallow grooves of any shape, by a perturbation method, and the limit solution for transverse flow over infinitely deep grooves, by the Wiener–Hopf method.

4.1. *Series solution for shallow grooves*

If we consider a shallow wall profile of the form $y = \epsilon y_0(x)$ the solution of either (2a) or (3a) can be expanded in a power series in ϵ as

$$w = w^{(0)} + \epsilon w^{(1)} + \epsilon^2 w^{(2)} + \ldots; \quad \psi = \psi^{(0)} + \epsilon \psi^{(1)} + \epsilon^2 \psi^{(2)} + \ldots. \tag{6}$$

The differential equation for each term of the series remains (2a) or (3a)

respectively, since these equations are linear. The boundary conditions for longitudinal flow (2*b*) after expansion give

$$w^{(0)}(x,0)=0; \quad w_y^{(0)}(x,\infty)=1, \tag{7a}$$

$$w^{(1)}(x,0)+w_y^{(0)}(x,0)\,y_0(x)=0; \quad w_y^{(1)}(x,\infty)=0, \tag{7b}$$

$$w^{(2)}(x,0)+w_y^{(1)}y_0+\tfrac{1}{2}w_{yy}^{(0)}y_0^2=0; \quad w_y^{(2)}(x,\infty)=0, \tag{7c}$$

and so on. (The expansion can be continued to all orders.)

The solution can then be expressed, for any given wall profile $y_0(x)$, in terms of the Fourier series expansions of y_0 and w. Denoting by Y_n the Fourier coefficients of the expansion of $y_0(x)$ (periodic of period 2π by assumption) and using the expansion of w given in (4) we obtain that $w^{(0)}(x,y)=y$, and

$$a_n^{(0)}=0; \quad a_n^{(1)}=-Y_n; \quad a_n^{(2)}=-\sum_{m=-\infty}^{\infty}|m|\,Y_m\,Y_{n-m}. \tag{8}$$

Since $h_\parallel=a_0$, we can immediately write the expression of the longitudinal protrusion height, to second order in ϵ, as

$$h_\parallel \sim -\epsilon Y_0-2\epsilon^2\sum_{m=1}^{\infty}m|Y_m|^2, \tag{9}$$

where we made use of the fact that, $y_0(x)$ being real, $Y_{-m}=Y_m^*$ (the complex conjugate of Y_m).

For cross-flow we proceed analogously. The boundary conditions (3*b*) after expansion become

$$\psi^{(0)}(x,0)=0; \quad \psi_y^{(0)}(x,0)=0; \quad \psi_{yy}^{(0)}(x,\infty)=1, \tag{10a}$$

$$\psi^{(1)}(x,0)+\psi_y^{(0)}y_0=0; \quad \psi_y^{(1)}(x,0)+\psi_{yy}^{(0)}y_0=0; \quad \psi_{yy}^{(1)}(x,\infty)=0, \tag{10b}$$

$$\psi^{(2)}(x,0)+\psi_y^{(1)}y_0+\tfrac{1}{2}\psi_{yy}^{(0)}y_0^2=0;$$

$$\psi_y^{(2)}(x,0)+\psi_{yy}^{(1)}y_0+\tfrac{1}{2}\psi_{yyy}^{(0)}y_0^2=0; \quad \psi_{yy}^{(2)}(x,\infty)=0, \tag{10c}$$

and so on. On introducing the Fourier expansions of y_0 and ψ, the latter according to (5), the solution of (10) gives $\psi^0(x,y)=\frac{1}{2}y^2$, and

$$A_n^{(0)}=B_n^{(0)}=0, \tag{11a}$$

$$A_n^{(1)}=0; \quad B_n^{(1)}=-Y_n, \tag{11b}$$

$$A_n^{(2)}=\frac{1}{2}\sum_{m=-\infty}^{\infty}Y_m\,Y_{n-m}; \quad B_n^{(2)}=|n|\,A_n^{(2)}-2\sum_{m=-\infty}^{\infty}|m|\,Y_m\,Y_{n-m}, \tag{11c}$$

whence

$$h_\perp=B_0\sim-\epsilon Y_0-4\epsilon^2\sum_{m=1}^{\infty}m|Y_m|^2. \tag{12}$$

We note that both protrusion heights are given at first order by the negative mean value of $y_0(x)$; in other words the effective plane walls seen by longitudinal flow and cross-flow are both approximately located on the mean line through the corrugated wall. An interesting consequence is that the height difference $h_\parallel-h_\perp$ has a quadratic expression:

$$\Delta h=2\epsilon^2\sum_{m=1}^{\infty}m|Y_m|^2. \tag{13}$$

Equation (13) gives a positive value for any wall shape $y_0(x)$, so that the effective wall seen by cross-flow is always located above the one seen by longitudinal flow, the

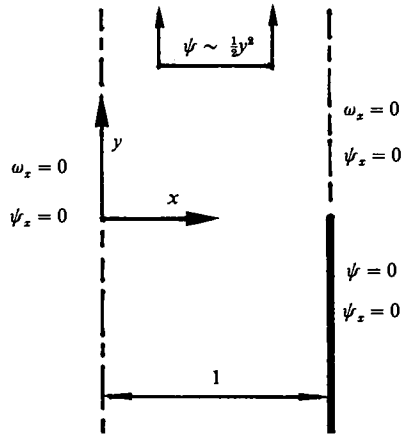

FIGURE 5. The infinitely-deep-groove problem.

condition under which a greater resistance is offered to cross- than to longitudinal flow. On the other hand, Δh is a second-order quantity in ϵ, and therefore the effect is very small for shallow grooves.

4.2. *The limit of infinitely deep grooves*

A wall with infinitely deep grooves may be represented as an array of parallel infinitely thin half-plates, or blades, the edges of which are grazed by the fluid stream. The solution of the longitudinal-flow problem (2) for this geometrical configuration can be obtained through a conformal mapping, as reported by Bechert & Bartenwerfer (1989). The resulting protrusion height is finite, despite the infinite depth of the grooves, and once normalized to the period is given by

$$\bar{h}_{\parallel} = \pi^{-1} \log 2 = 0.220\,635\ldots. \tag{14}$$

We shall now solve the cross-flow problem (3) for the infinite-groove wall configuration by the Wiener–Hopf method along the lines of Luchini (1991), where the Stokes flow out of an array of semi-infinite plane ducts was calculated. On comparing the present problem with the one considered by Luchini (1991), we notice that the geometrical configuration is the same but the boundary conditions are different: the main flow is directed perpendicular to the plates rather than coming out between them.

In order to formulate the Wiener–Hopf problem, we consider a single half-period of the flow, which for the scope of this section will be located in the strip $0 \leqslant x \leqslant 1$ rather than $0 \leqslant x \leqslant \pi$. The conditions holding at the boundary of a half-period follow from symmetry considerations and are indicated in figure 5.

If boundary conditions of the same type were imposed for $-\infty < y < \infty$ this problem could be solved by Fourier-transforming with respect to the y-coordinate. Indeed, on introducing the Fourier transform of ψ as

$$\Psi(x,k) = \int_{-\infty}^{\infty} \psi(x,y)\, \mathrm{e}^{-\mathrm{i}ky}\, \mathrm{d}y \tag{15}$$

and the Fourier transform $\Omega(x,k)$ of ω analogously, we can easily write the transformed solution of $(3a)$ as

$$\Psi(x,k) = [A(k) + B(k)\,x]\,\mathrm{e}^{-kx} + [C(k) + D(k)\,x]\,\mathrm{e}^{kx}. \tag{16}$$

The two conditions $\Psi_x(0,k)=0$ and $\Omega_x(0,k)=0$ select a solution that is even with respect to x:

$$\Psi(x,k)=2A(k)\cosh kx-2\mathrm{i}B(k)\,x\sinh kx. \tag{17}$$

If now, in addition to the condition $\psi_x(1,y)=0$, $\psi(1,y)$ were known for all y, we could determine the remaining two coefficients A and B, and write

$$\Psi(x,k)=\frac{(\sinh k+k\cosh k)\cosh kx-kx\sinh k\sinh kx}{\sinh k\cosh k+k}\Psi(1,k). \tag{18}$$

In particular, $\Omega_x(1,k)$ would then be given by

$$\Omega_x(1,k)=-\frac{2k^3\sinh^2 k}{\sinh k\cosh k+k}\Psi(1,k). \tag{19}$$

In fact we do not know $\psi(1,y)$ for all y. Instead we have the two conditions $\psi(1,y)=0$ for $-\infty<y<0$ and $\omega_x(1,y)=0$ for $0<y<\infty$. Determining two functions satisfying these conditions and whose transforms are related by a linear equation such as (19) constitutes what is called a Wiener–Hopf problem, and can be solved by Hilbert's factorization method.

The key to Hilbert's method is the observation that the Fourier transform of a function that is zero for $y<0$ is an analytic function of the complex variable k in the half-plane $\mathrm{Im}\,(k)<0$, as follows directly from its definition (15), and conversely the transform of a function that is zero for $y>0$ is analytic in the half-plane $\mathrm{Im}\,(k)>0$. Therefore what we have to do is split the coefficient of $\Psi(1,k)$ in (19) in the ratio of two factors, one analytic in the half-plane $\mathrm{Im}\,(k)<0$ and the other in the half-plane $\mathrm{Im}\,(k)>0$. This factorization can be obtained by taking logarithms of both sides and then applying Cauchy's formulae, which give two functions, one analytic in the upper and the other in the lower half-plane, whose *difference* is given.

In the present case it is convenient first to factor out the fourth-order zero that the coefficient of (19) has in the origin. Then we can write

$$\frac{\Omega_x(1,k)}{\Psi(1,k)}=-k^4\frac{N(k)}{D(k)}, \tag{20}$$

where

$$\log N(k)=\frac{1}{2\pi\mathrm{i}}\int_{-\infty}^{\infty}\log\left[\frac{2\sinh^2 k'}{k'(\sinh k'\cosh k'+k')}\right]\frac{\mathrm{d}k'}{k'-k-\mathrm{i}0}, \tag{21}$$

$$\log D(k)=\frac{1}{2\pi\mathrm{i}}\int_{-\infty}^{\infty}\log\left[\frac{2\sinh^2 k'}{k'(\sinh k'\cosh k'+k')}\right]\frac{\mathrm{d}k'}{k'-k+\mathrm{i}0}. \tag{22}$$

(The symbol $+\mathrm{i}0$ ($-\mathrm{i}0$) indicates that the denominator must be given a small positive (negative) imaginary part which is then let go to zero after calculating the integral.)

The solution of the Wiener–Hopf problem is now given by

$$\Omega_x(1,k)=-k^{\alpha}P(k)N(k),\quad \Psi(1,k)=k^{\beta}P(k)D(k),$$

where $\alpha-\beta=4$ and $P(k)$ is an arbitrary polynomial, which must be determined from the behaviour at infinity and near the origin of the particular solution required. In the present case, no polynomial must be included if we want the singularity that the solution has at the origin of the y-axis (the blade tip) to be of the lowest possible order, and β must equal -3, since we want ψ to behave as y^2 for $y\to\infty$. More precisely, from the relations between the behaviour near zero of transforms and the

behaviour at infinity of the transformed functions we know that, if $\psi \sim \frac{1}{2}y^2$ for $y \to \infty$, $\Psi \sim \mathrm{i}k^{-3}$ for $k \to 0$. We thus obtain

$$\Psi(1, k) = \mathrm{i}k^{-3}D(k), \tag{23}$$

with $D(k)$ given by (22). It might be thought that (23) should be further divided by $D(0)$, but in the present case we know that $D(0) = 1$ because the function to be factored, the argument of the logarithm that appears under the integral sign in (22), is an even real function of k which takes the value 1 in the origin (see Luchini 1991 for the complete argument applied to a similar case).

Equations (22) and (23) together with (18) formally solve the problem completely. Although (22) still contains a convolution integral which cannot be calculated analytically, this integral can be calculated through numerical Fourier transforms, if the complete flow pattern is desired, in a manner analogous to that used by Luchini (1991).

In order to calculate the cross-flow protrusion height it is sufficient to continue the relation between the asymptotic behaviour for $y \to \infty$ of ψ and the behaviour near zero of its transform to its second term. In fact, it follows from general theorems of the theory of Fourier and Laplace transforms that if $\psi \sim \frac{1}{2}y^2 + h_\perp y$ for $y \to \infty$ (which is the definition of the protrusion height $h_\perp$), then $\Psi \sim \mathrm{i}k^{-3} - h_\perp k^{-2}$ for $k \to 0$. Therefore

$$h_\perp = -\mathrm{i}\left[\frac{\mathrm{d}D}{\mathrm{d}k}\right]_{k=0} = -\mathrm{i}\left[\frac{\mathrm{d}(\log D)}{\mathrm{d}k}\right]_{k=0}, \tag{24}$$

where the last equality follows because $D(0) = 1$. Differentiating (22) under the sign of integral we thus obtain

$$h_\perp = -\frac{1}{2\pi}\int_{-\infty}^{\infty} \log\left[\frac{2\sinh^2 k'}{k'(\sinh k' \cosh k' + k')}\right]\frac{\mathrm{d}k'}{k'^2} \tag{25}$$

where the symbol $+\mathrm{i}0$ has been omitted because the integral is actually regular (the logarithm vanishes as k'^2 in the origin).

The integral of (25) can easily be evaluated numerically. Once normalized to the period (which in this section is 2) the cross-flow protrusion height for infinitely deep grooves turns out to be $\bar{h}_\perp = \frac{1}{2}h_\perp = 0.0885657\ldots$.

Combining the last result with (14) finally gives $\overline{\Delta h} = 0.132069\ldots$.

5. The numerical method

In order to calculate the two protrusion heights numerically for a general wall profile, we have developed a boundary-element computer code which solves the Laplace and the biharmonic equation in a half-plane-like domain bounded by a periodic wall.

The algorithm is based on the periodic Green function, rather than the free-space Green function generally adopted in boundary-element method codes, so that the calculation may be restricted to a single period of the wall profile.

Both wall shape and unknowns, that is the boundary values of velocity and stream function and their normal derivatives, are approximated by piecewise polynomials, and the boundary integrals appearing in Green's formula are computed by a Gauss–Legendre integration formula modified so as to take into account the logarithmic singularity of the Green function. The order of accuracy of the integration formula is preserved by subtracting the singular logarithmic contribution

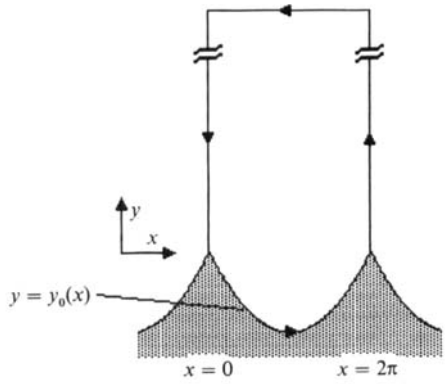

FIGURE 6. Integration contour for the boundary-integral formulation.

and integrating it analytically in the appropriate subintervals. The problem is thus reduced to a, nearly singular, algebraic system of N linear equations. The integral constraint resulting from the Neumann condition on normal derivative is handled by a pseudo-variational formulation which de-singularizes the system through the introduction of an additional unknown, and the solution is then found by direct Gauss elimination. The protrusion height is expressed as another boundary integral which is again computed by Gauss–Legendre integration.

The biharmonic equation is solved by first reformulating the problem as two Laplace equations with coupled boundary conditions and then discretizing the boundary integrals that represent these two equations in the manner described above. The procedure involves the inversion of only one $N \times N$ matrix, in addition to the one already inverted in solving the Laplace equation, rather than the much slower inversion of a $2N \times 2N$ matrix which would be entailed by a direct boundary-element formulation of the biharmonic equation in terms of its own Green function.

5.1. *The boundary-element integral equation for the Laplace equation*

All boundary-element algorithms for the Laplace equation are based on Green's formula,

$$f(\boldsymbol{r}') = \oint \left[f(\boldsymbol{r}) \frac{\partial G}{\partial n}(\boldsymbol{r}, \boldsymbol{r}') - G(\boldsymbol{r}, \boldsymbol{r}') \frac{\partial f}{\partial n}(\boldsymbol{r}) \right] \mathrm{d}s, \tag{26}$$

which gives the value at any point $\boldsymbol{r}'$ of a general solution f in terms of the values taken by f and its normal derivative on the boundary of the solution domain (spanned by the curvilinear abscissa s). In (26) the Green function G is, by definition, any one solution of the Poisson equation $\nabla^2 G = \delta|\boldsymbol{r} - \boldsymbol{r}'|$; different formulations will result from different choices of the Green function.

In the present case, in which we are dealing with a periodic corrugated wall, it is useful to enforce periodicity directly by choosing a periodic Green function. We may then take a single period as solution domain and apply (26) to the contour shown in figure 6, formed by one period of the wall, two straight lines parallel to the y-axis, say $x = 0$ and $x = 2\pi$, and a line joining these two at $y = +\infty$; if both f and G are periodic the contributions to (26) from the two lines $x = 0$ and $x = 2\pi$ cancel each other and an obvious simplification ensues. A periodic solution of the Poisson equation suitable for this purpose may easily be determined by conformal-mapping techniques. More than one choice is possible; of these the simplest is probably

$$G(\boldsymbol{r}, \boldsymbol{r}') = (4\pi)^{-1} \log \left[\cosh (y - y') - \cos (x - x') \right].$$

We have thus eliminated the contributions to (26) from the lateral boundaries of the solution domain. We can, in addition, eliminate the contribution from the line at infinity if we choose a Green function which vanishes for $y \to \infty$. This effect can be obtained by subtracting from the previous Green function its asymptotic behaviour, i.e. $(4\pi)^{-1}(y-y'-\log 2)$. The result is

$$G(\boldsymbol{r},\boldsymbol{r}') = (4\pi)^{-1}\{\log[2\cosh(y-y')-2\cos(x-x')]-y+y'\}. \tag{27}$$

Adopting this Green function we can use (26) with the line integral extended over one wall period alone. We shall also find useful to have x as the integration variable along the wall, and therefore we rewrite (26) as

$$f(x',y') = \int_0^{2\pi}\left\{f[x,y_0(x)]\frac{\partial G}{\partial n}\frac{\mathrm{d}s}{\mathrm{d}x}-G(x-x',y-y')\,\varphi(x)\right\}\mathrm{d}x, \tag{28}$$

where $\varphi(x) = (\partial f/\partial n)[x,y_0(x)]\,(\mathrm{d}s/\mathrm{d}x)$.

According to the general philosophy of boundary-element methods, we now particularize (28) to $y' \to y_0(x')$ (with some care needed in taking the limit from the interior) and interpret the result as an integral equation relating the two functions $f[x,y_0(x)]$ and $\varphi(x)$, either one of which may be the unknown.

5.2. *The Gaussian-integration Galerkin procedure*

For the discretization of the integral equation we have devised a piecewise-polynomial technique which can be enacted at low or high orders of approximation with essentially the same ease.

The two main ingredients of this technique are the representation of f and φ through piecewise polynomials and the adoption of a Gaussian integration formula for all the required integrals. Let the interval $(0,2\pi)$ be divided into N, generally non-uniform, subintervals (x_i, x_{i+1}). In each subinterval we assume every unknown, say φ, to be represented by a polynomial of order $M-1$, and approximate the integral of this polynomial times the Green function by an M-point Gaussian formula, i.e. by the sum of the values taken by the integrand at M purposely chosen points, multiplied by suitable weights. The key property of Gaussian integration, which is also exploited in other numerical techniques such as the spectral-element method for partial differential equations, is that it is exact for polynomials up to order $2M-1$, so that we are effectively approximating the Green function through a polynomial of order M in each subinterval. At the same time, we do not need to deal with the polynomial representation of φ explicitly, because we can simply adopt as variables the values of φ at the M Gaussian integration points in each subinterval, and never let the M coefficients of the polynomial appear at all.

The discretization of (28) along the axis x' is achieved by first recasting the equation in weak form, that is multiplying it by a test function $T(x')$ and integrating over $(0,2\pi)$, and then discretizing this new integral in the same way as the previous one. Then, requiring the equation to be satisfied for T being any piecewise polynomial of order $M-1$ over the chosen partition into N intervals gives a finite linear system of order MN as the discrete representation of the integral equation.

The effect obtained through the use of Gaussian integration on a number of points equal to the number of coefficients of the polynomial representation of the unknowns is that the procedure, although conceptually of the Galerkin type, can in practice be implemented as a collocation technique using the zeros of Legendre polynomials as collocation points, without calculating any numerical integrals at all. The property

of Gaussian integration of being exact for polynomials up to order $2M-1$ ensures that the Green function is implicitly interpolated to a consistent order.

The basic technique illustrated above, valid for a generic integral equation, must be modified slightly in the case of (28) because the kernel, either G or $\partial G/\partial n$, is singular at $x = x'$, so that the possibility of representing it locally by a polynomial fails, and at the same time the value of the kernel for $x = x'$, required in the integration formula, is infinite. This difficulty has been eliminated by isolating the singular contribution to the kernel of each integral and integrating numerically the regular part only, and analytically the product of the singular part with the polynomials that represent φ and T over the relevant subinterval. This calculation need be done only once, and the result, obtained at first as a bilinear function of the coefficients of the polynomial representations of φ and T, may be recast once and for all as a bilinear function of the values taken by these polynomials at the Gaussian points.

5.3. *Dealing with the singularity of the integral equation*

As is often the case for boundary integrals derived from the Laplace equation, the integral equation (28) is a singular one, in the sense that it admits a non-zero solution with a zero known term and conversely is not guaranteed to have finite solutions unless the known term satisfies a condition. When it does have a solution, this is not unique unless an additional condition is imposed. This behaviour, analogous to that of a linear system with a coefficient matrix of rank deficient by one, is a consequence of the well-known property of the solutions of the Laplace equation that the integral over a closed boundary of $\partial f/\partial n$ must be zero. The reason why this is a complication is that the matrix obtained as the discrete representation of the integral equation will be nearly singular but, because of discretization errors, not quite so. The problem is then that of obtaining a solution which satisfies an additional condition, as the exact solution of the continuous problem does, and only approximately satisfies the nearly singular linear system obtained from the discretization.

In particular, in the physical problem we are concerned with, the additional condition that must be satisfied by φ corresponds to the imposition of the velocity gradient at infinity; the contributions of the sides to the boundary integral of $\partial w/\partial n$ cancel each other and the contribution of infinity, where $\partial w/\partial y$ is constant and equal to 1, is 2π. We thus obtain the condition that

$$\int_0^{2\pi} \varphi \, \mathrm{d}x = \int_{\text{wall}} \frac{\partial w}{\partial n} \mathrm{d}s = -2\pi. \tag{29}$$

The simplest approach to the above problem is dictated by the ordinary theory of rank-deficient linear systems: simply drop one of the equations (which are linearly dependent) and replace it by the additional condition. This operation yields a new non-singular system and in principle works also when, owing to discretization errors, the system is not exactly singular, the effect being in this case that the dropped equation will not be satisfied exactly. However, eliminating the singularity in this manner introduces an unwarranted asymmetry, since any one equation chosen to be dropped will correspond to a particular point on the wall which is not otherwise special, and in practice may be observed to yield poor results.

A more symmetric approach, suggested by the analogy with a related variational problem, is to add a constant λ to the right-hand side of (28) and regard λ as a new unknown to be determined simultaneously with $\varphi(x)$ under the additional constraint (29). Doing so effectively de-singularizes the system; for the solution is unique, owing

to the explicitly imposed additional constraint, and exists for no matter which known term, the difference being that when the known term is compatible with the original equation, λ turns out to be zero in the solution, whereas when the known term is not compatible it does not. The discretization of this modified integral equation yields a finite system of $MN+1$ equations (one of which is the additional constraint (29)) in $MN+1$ unknowns (one of which is λ) which is definitely non-singular and may be solved by any standard method. After the solution, the smaller the value of λ turns out to be the better the approximation of the original integral equation by its discretized counterpart is.

5.4. *Calculation of the longitudinal protrusion height*

In order to apply the above technique to problem (2), longitudinal flow over a grooved surface, we need only insert the boundary condition $w[x, y_0(x)] = 0$ into (28), that is solve the homogeneous problem for φ under the constraint (29). Having done so, we can determine the longitudinal protrusion height by applying (28) again, but this time in the limit for $y' \to +\infty$. Since G tends to $(y'-y)/2\pi$ and w to $y'+h_\parallel$ in this limit, we easily obtain

$$\bar{h}_\parallel = \frac{h_\parallel}{2\pi} = \frac{1}{(2\pi)^2}\int_0^{2\pi} y_0(x)\,\varphi(x)\,\mathrm{d}x, \tag{30}$$

which can be discretized, consistently with the other integrals, by piecewise Gaussian integration.

5.5. *The boundary-element formulation of the biharmonic equation*

For problem (3), transverse flow, one possibility would be to set up a boundary-element formulation based on the Green function of the biharmonic equation, and thus obtain a system of $2MN$ equations in $2MN$ unknowns by imposing the two boundary conditions at the wall; however, we can instead reduce the problem to two coupled Laplace equations, which we can solve by the successive inversion of two $MN \times MN$ matrices one of which is in common with the previous problem. It is well known (and very easily verified) that if f and g are harmonic functions, $\psi = yf+g$ is a solution of the biharmonic equation. With this substitution, boundary conditions (3*b*) may be rewritten as

$$y_0(x) f[x, y_0(x)] + g[x, y_0(x)] = 0, \tag{31a}$$

$$y_0 \frac{\partial f}{\partial n} + \frac{\partial g}{\partial n} + \hat{\boldsymbol{n}}\cdot\hat{\boldsymbol{y}} f[x, y_0(x)] = 0 \tag{31b}$$

(where $\hat{\boldsymbol{n}}\cdot\hat{\boldsymbol{y}}$ is the product of the two unit vectors corresponding to the outward normal and the y-axis). Condition (3*c*) may be translated into $f_y(x, \infty) = \frac{1}{2}$, $g_y(x, \infty) = 0$ (the latter condition is actually arbitrary; 0 is assumed for convenience).

Let us now assume $f[x, y_0(x)]$ as the main unknown. Equation (31*a*) directly gives us $g[x, y_0(x)]$ in terms of f. On the other hand, the solution of the boundary-integral equation for the Laplace equation gave us the discrete representation as a matrix of the linear operator $\tilde{\mathrm{L}}$ relating the values on the boundary of a harmonic function and its normal derivative, so that

$$\frac{\partial f}{\partial n} = \tilde{\mathrm{L}}(f) + \tfrac{1}{2} f_{n0}; \quad \frac{\partial g}{\partial n} = \tilde{\mathrm{L}}(g) \tag{32}$$

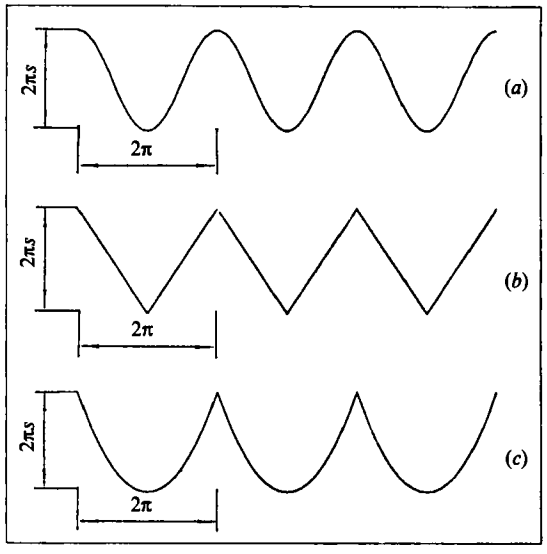

FIGURE 7. Groove shapes chosen for numerical analysis: (*a*) cosinusoidal, (*b*) triangular, (*c*) parabolic.

(with f_{n0} denoting the solution of the problem with $f[x, y_0(x)] = 0$ and $f_y(x, \infty) = 1$ and $\tilde{\mathrm{L}}(f)$ that of the problem with $f[x, y_0(x)]$ arbitrary and $f_y(x, \infty) = 0$). Inserting these expressions into (31*b*) we obtain

$$y_0 \tilde{\mathrm{L}}(f) - \tilde{\mathrm{L}}(y_0 f) + \hat{\boldsymbol{n}} \cdot \hat{\boldsymbol{y}} f = -\tfrac{1}{2} y_0 f_{n0}, \tag{33}$$

which, in discretized form, is a linear system of order MN from which f may be determined.

Once this is done, the transverse protrusion height is given by the expansion at infinity of $f(x, y)$ alone (because we have imposed the condition $g_y(x, \infty) = 0$) as $f \sim \frac{1}{2}y + h_\perp$. A formula analogous to (30) gives

$$\bar{h}_\perp = \frac{h_\perp}{2\pi} = \frac{1}{(2\pi)^2} \int_0^{2\pi} \left(y_0(x) f_n \frac{\mathrm{d}s}{\mathrm{d}x} + f \right) \mathrm{d}x. \tag{34}$$

6. Numerical results

6.1. *Performance of the numerical algorithm*

In order to test the performance of our algorithm, with particular regard to the use of higher approximations, we have considered two geometries: a cosinusoidal wall with a height equal to the period, and an array of parabolic grooves, again with a height equal to the period (shapes *a* and *c* of figure 7).

For the cosinusoidal profile a uniform spacing has been used. Figure 8 reports, on a bilogarithmic scale, the error in the calculation of $h_\parallel$ and $h_\perp$ versus the number of discretization points (the error being calculated with respect to a value obtained with a number of discretization points higher than all those appearing in the plot). Although the curves do not display the change in slope that one would expect in going from lower to higher orders of approximation, the error does decrease with increasing M, smoothly for $h_\parallel$ and somewhat more irregularly for $h_\perp$, losing roughly a factor of 20 in going from $M = 1$ to $M = 5$.

The parabolic-groove profile, with its pointed corners, constitutes a much tougher

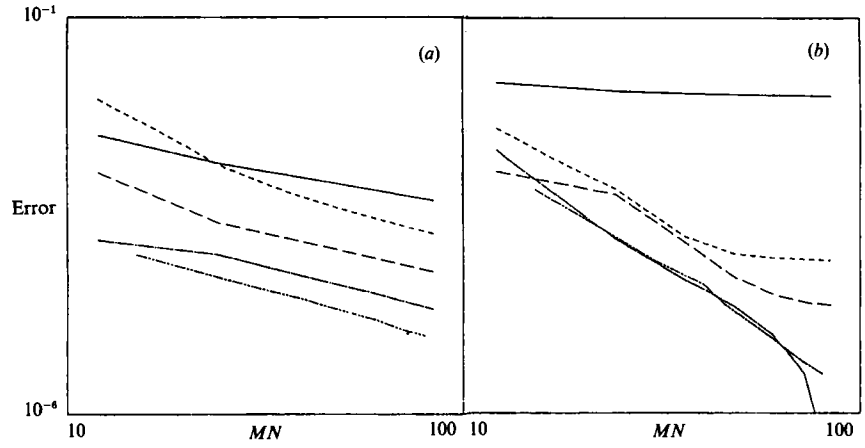

FIGURE 8. Bilogarithmic plot of the error in the calculation of (a) $h_{\parallel}$ and (b) $h_{\perp}$ versus the number of discretization points for a cosinusoidal-groove profile. The order of approximation is denoted as follows: ——, $M = 1$; – – – –, $M = 2$; — — —, $M = 3$; —·—·—, $M = 4$; —··—··—, $M = 5$.

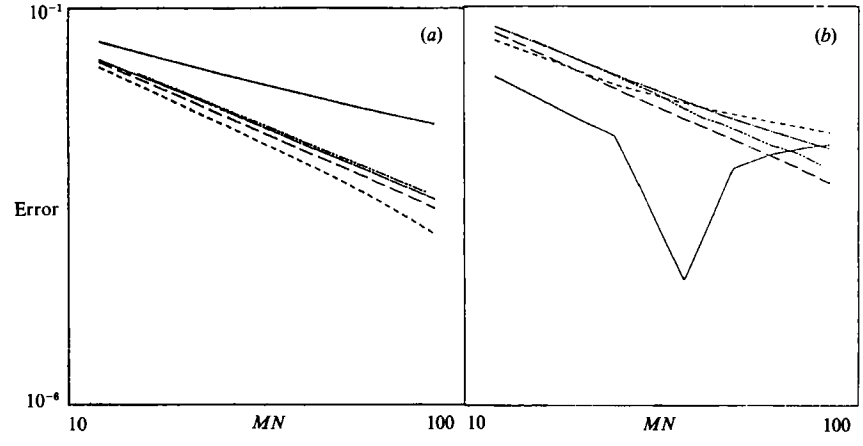

FIGURE 9. Bilogarithmic plot of the error in the calculation of (a) $h_{\parallel}$ and (b) $h_{\perp}$ versus the number of discretization points for a parabolic-groove profile with pointed corners. Order of approximation denoted as in figure 8.

test for the numerical algorithm, because near the corners the solution is non-analytic and thus not representable by polynomials, but is interesting in the applications. Nevertheless, although larger than that obtained for the cosinusoidal profile, the absolute error generated in the range of, say, $50 \leqslant MN \leqslant 100$ is as low as needed for practical applications (provided a non-uniform discretization is used with a much closer spacing near the corners). Figure 9 shows the errors of the computations performed with different values of M. Not surprisingly, the higher approximations do not perform very well in this test, and in fact turn out to worsen slightly with increasing M. It is interesting to observe, however, that in determining $h_{\parallel}$, $M = 2$ performs better than all the others, whereas in determining $h_{\perp}$, $M = 3$ is best. Either of these two is definitely better than $M = 1$ and therefore to be preferred to a simple piecewise-constant panel approach, even in the presence of corners.

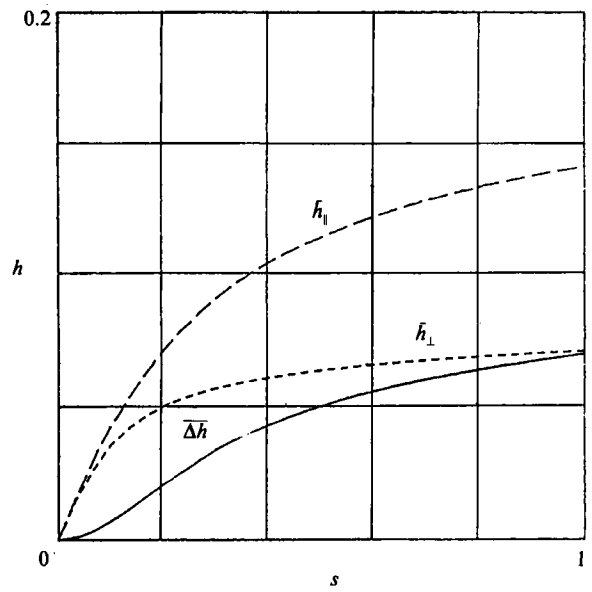

FIGURE 10. Parallel (– – –) and cross (———) protrusion heights and their difference (——) *vs.* depth for the cosinusoidal-groove profile.

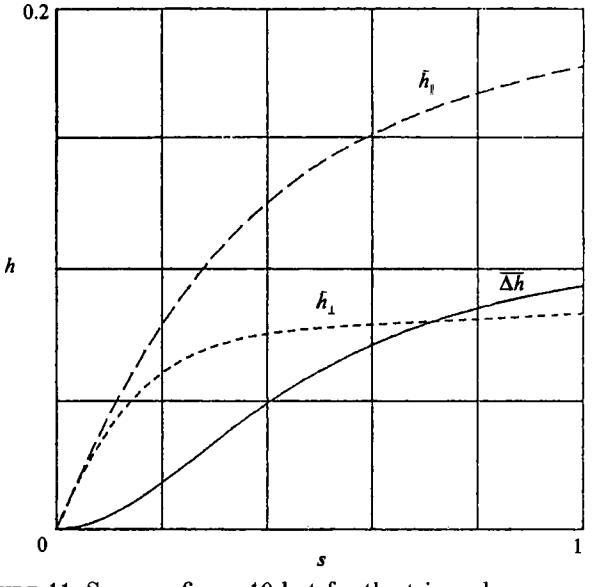

FIGURE 11. Same as figure 10 but for the triangular-groove profile.

6.2. *Analysis of the relative performance of different groove profiles*

Three groove geometries have been considered: sinusoidal, triangular and parabolic (figure 7), each for values of the ratio of height to period varying between zero and one. Figures 10–12 report the plots of the two protrusion heights and their difference versus the ratio of height to period s in each case. In all three cases it can be noticed that for $s \approx 0$ the curves of $\bar{h}_{\parallel}$ and $\bar{h}_{\perp}$ are tangent to each other while $\overline{\Delta h}$ goes to zero quadratically, in accordance with the results of §4.1, whereas for $s \to \infty$ the three curves tend to the limit values calculated in §4.2. The rate at which the limit is

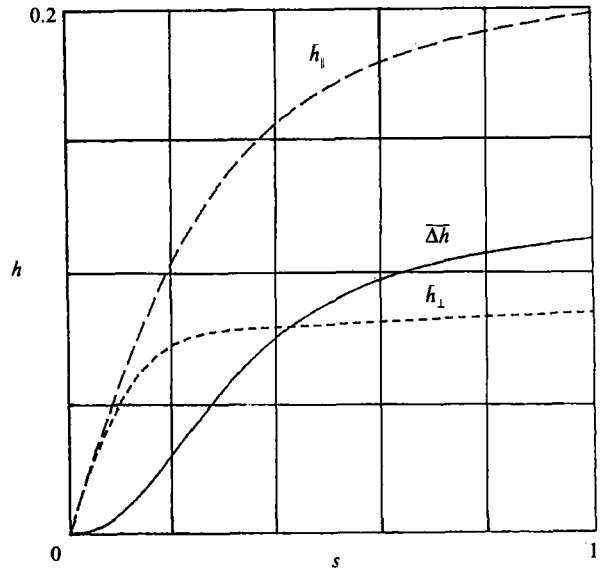

FIGURE 12. Same as figure 10 but for the parabolic-groove profile.

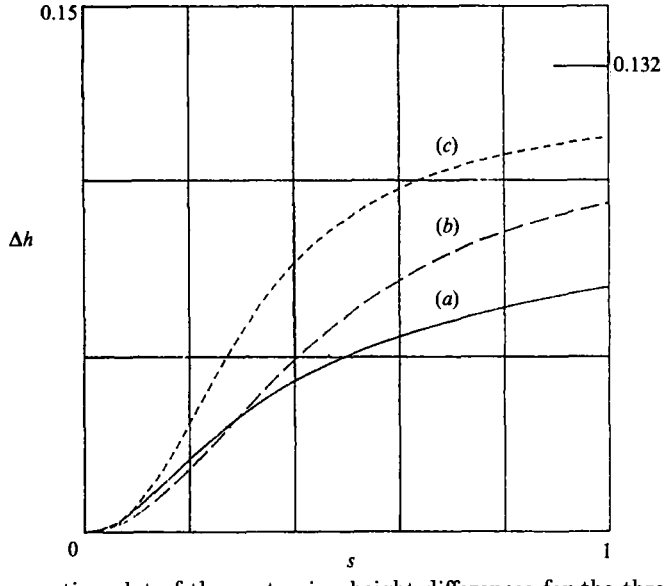

FIGURE 13. Comparative plot of the protrusion-height differences for the three groove profiles: (*a*) cosinusoidal, (*b*) triangular, (*c*) parabolic.

approached is, however, different. In fact, at $s = 1$ the parabolic profile has already attained 85% of the limit value of the protrusion height difference $\overline{\Delta h}$, whereas the triangular profile has attained 72% and the sinusoidal profile only 53%. The three plots of $\overline{\Delta h}$ are reported together, for comparison, in figure 13.

Nevertheless, all three groove profiles are bound to reach the limit for a sufficiently large depth; in addition, it is interesting to observe that in all three cases the increase of all three parameters $h_\parallel$, $h_\perp$ and Δh is monotonic, so that, in particular, intermediate values higher than the limit never occur. It may also be noticed that the curve of $h_\perp$ approaches the limit and becomes flat appreciably earlier than the curve of $h_\parallel$,

appearing to indicate that parallel flow penetrates deeper into the grooves and thus 'sees' the bottom longer than cross-flow. This observation is, of course, in agreement with the fact that the parallel protrusion height itself is larger than the transverse one.

7. Conclusions

Our main aim in undertaking this study was to substantiate quantitatively the intuitive notion that a grooved surface offers a greater resistance to cross- than to parallel flow, which underlies the generally accepted explanation of why a grooved surface can reduce turbulent drag. Indeed, whereas the effects of the grooved surface on a parallel viscous flow have been extensively studied in the past, its effects on cross-flow, although recently measured experimentally (Bechert *et al.* 1990), do not seem to have ever been calculated.

Our analysis of the Stokes flow of a fluid across the grooves of the surface allows a quantitative characterization of the differential effect of the wall on parallel flow and cross-flow in terms of the difference of two protrusion heights. In fact, both parallel flow and cross-flow turn, at some distance from the wall, into uniform shear flows, similar to those which exist in proximity of a plane wall, and the only remaining memory of the existence of a solid surface is in the location of the virtual plane wall from which the velocity profile appears to originate. Therefore, as far as the main stream is concerned, a corrugated wall with a thickness not exceeding that of the viscous sublayer is equivalent to a plane wall in a suitable position. What makes the corrugated wall effective in retarding cross-flow, however, is that the virtual plane wall seen by cross-flow is located deeper into the fluid than the one seen by parallel flow, thus giving rise to a greater resistance. The only parameter that remains in the outer stream to differentiate a corrugated from a true plane wall is just the distance between the two virtual plane walls, that is the difference of the two protrusion heights Δh. We have been able to prove that this parameter is positive for shallow corrugations of any shape and is again positive for infinitely deep corrugations; there is numerical evidence that it is probably always positive.

We thus have a parameter that quantitatively qualifies the effectiveness of a given corrugation profile in inhibiting cross-flow. Previously, in the absence of a quantitative calculation of cross-flow inside the viscous sublayer, the role of such a parameter was played by the parallel protrusion height $h_{\parallel}$ alone, that is by the distance between the riblet tips and the parallel virtual wall rather than between the two virtual walls, a choice that is equivalent to assuming that cross-flow does not penetrate at all below the riblet tips. Actually, our calculations show that cross-flow penetrates, roughly speaking, half as deep as parallel flow, at least for sufficiently deep grooves. For shallow grooves we have the unforeseen result that the parallel and cross protrusion heights are of the same order of magnitude and their difference is only second order in groove depth.

The second aim of our work was to provide a tool to calculate the above parameter, the protrusion height difference, for several groove shapes, and possibly optimize the shape with the aid of such a tool. We have developed an analytic theory of limiting behaviours and a numerical program that calculates the protrusion heights of arbitrary shapes.

On the analytical side, we have been able to solve the limiting case of very shallow grooves by series expansion and the one of infinitely deep grooves by the Wiener–Hopf method.

On the numerical side, we have obtained an algorithm which can easily work at high orders of approximation and, when the surface profile is smooth, offers a significantly better performance than an ordinary piecewise-constant-panel method (to which it more or less reduces for $M = 1$). For pointed profiles performance is not as good, as may easily be expected, but still $M = 2$ or 3 is about an order of magnitude better than $M = 1$.

The numerical algorithm has been applied to the analysis of several groove profiles. The answer to the optimization problem is, however, trivial, at least as long as no external constraints are imposed: the maximum protrusion height difference for a given period is attained by infinitely deep grooves, the case that was analysed in §4.2.

In general our results confirm the trend of pointed profiles providing better results, for equal depth, than smooth ones, in accordance with the conclusions reached by Bechert & Bartenwerfer (1989) on the basis of their analysis of the parallel protrusion height alone. Our results for the transverse protrusion height are in agreement with the values obtained by Bechert *et al.* (1990) from their elastic-plate analogy ($\bar{h}_\perp = 0.08 \pm 0.03$ for semicircular grooves and $\bar{h}_\perp = 0.075 \pm 0.03$ for equilateral-triangle grooves).

Finally, a comment may be made on the possible rise of recirculation regions inside the grooves. It is well known (Moffat 1964) that such recirculation regions, and in fact even infinite sequences of them, can arise in Stokes flow inside corners. Recirculation regions have indeed been observed by Bechert *et al.* (1990) in their high-viscosity cross-flow experiment; similar recirculation regions are present in numerical calculations and experimental visualizations of Stokes flow in rectangular cavities (Takematsu 1965; Taneda 1979) and would certainly have appeared in our calculations as well had we plotted the bulk behaviour of the stream function rather than restricting the calculation to the boundary only. However, we should be careful not to attach to these viscous eddies too much of the significance that is usually associated with high-velocity separating flows. They are the result of a linear phenomenon that takes place wherever velocity is so low that the Stokes equations are valid, and, since they are not convected with the stream, have hardly any bearing on the triggering mechanism of nonlinear instabilities and the overall balance of turbulent eddies.

This work was funded by the Italian Ministry of Public Education. Preliminary versions of parts of this paper were presented at the X AIMETA (Associazione Italiana di MEccanica Teorica e Applicata) Conference, Pisa 2–5 Oct. 1990, and at the IABEM-90 (International Association for Boundary-Element Methods) Symposium, Rome, 15–18 Oct. 1990.

REFERENCES

Baron, A., Quadrio, M. & Vigevano, L. 1989 Riduzione della resistenza di attrito in correnti turbolente e altezza di protrusione di pareti scanalate. In *Proc. X AIDAA Conf., Pisa, 16–20 October 1989*, pp. 92–100.

Bechert, D. W. & Bartenwerfer, M. 1989 The viscous flow on surfaces with longitudinal ribs. *J. Fluid Mech.* **206**, 105–129.

Bechert, D. W., Bartenwerfer, M. & Hoppe, G. 1990 Turbulent drag reduction by nonplanar surfaces – a survey on the research at TU/DLR Berlin. In *Proc. IUTAM Symp. on Structure of Turbulence and Drag Reduction, Zürich, 25–28 July 1989* (ed. A. Gyr), pp. 525–543. Springer.

BECHERT, D. W., BARTENWERFER, M., HOPPE, G. & REIF, W.-E. 1986 Drag-reduction mechanisms derived from shark skin. In *15th Congr. Intl Counc. Aeronautical Sciences, London 7–12 Sept. 1986, AIAA Paper* ICAS-86-1.8.3.

BECHERT, D. W., HOPPE, G. & REIF, W.-E. 1985 On the drag reduction of the shark skin. *AIAA Paper* 85-0546.

BURDAK, V. D. 1969 Function of the ctenoid apparatus of fish in the presence of a turbulent boundary layer. *Zool. Zh.* **48**, 1053–1055 (in Russian).

BUSHNELL, D. M. 1983 Turbulent drag reduction for external flows. *AIAA 21st Aerospace Sciences Meeting, Reno, Nevada, AIAA Paper* 83-0227.

CHERNYSHOV, O. B. & ZAYETS, V. A. 1970 Some peculiarities of the structure of the skin of sharks. In *Hydrodynamic Problems of Bionics*. Bionica Nr. 4, pp. 77–83 (in Russian).

CHOI, K. S. 1987 Test of drag reducing riblets on a one-third scale racing yacht. In *Proc. Turbulent Drag Reduction by Passive Means, R. Aero. Soc., London 15–17 Sept. 1987.*

LUCHINI, P. 1991 Solution of a coupled creeping-flow problem by the Wiener–Hopf method. *J. Engng Maths* **25**, 23–30.

MCLEAN, J. D., GEORGE-FALVY, D. N. & SULLIVAN, P. P. 1987 Flight-test of turbulent skin-friction reduction by riblets. In *Proc. Turbulent Drag Reduction by Passive Means, R. Aero. Soc., London 15–17 Sept. 1987.*

MOFFAT, H. K. 1964 Viscous and resistive eddies near a sharp corner. *J. Fluid Mech.* **18**, 1–18.

PREZIOSI, L., CHEN, K. & JOSEPH, D. D. 1989 Lubricated pipelining: stability of core-annular flow. *J. Fluid Mech.* **201**, 323–356.

SAWYER, W. G. & WINTER, K. G. 1987 An investigation of the effect on turbulent skin friction of surfaces with streamwise grooves. In *Proc. Turbulent Drag Reduction by Passive Means, R. Aero. Soc., London 15–17 Sept. 1987.*

TAKEMATSU, M. 1965 Viscous flow in a two-dimensional cavity. *J. Phys. Soc. Japan* **20**, 283.

TANEDA, S. 1979 Visualization of separating Stokes flows. *J. Phys. Soc. Japan* **46**, 1935–1942.

TRIGUI, N. & GUEZENNEC, Y. G. 1990 Turbulence modification by large eddy breakup devices in a passively heated turbulent boundary layer. In *ASME Forum on Turbulent Flows, Toronto 4–7 June 1990*, vol. FED-94, pp. 17–22. ASME.

WALSH, M. J. 1983 Riblets as a viscous drag reduction technique. *AIAA J.* **21**, 485–486.